2 PML Parameters and Convergence

2.1 Motivation and General Considerations

According to the FDFD method the analytical wave equation of electromagnetic (EM) fields, given by 2.1, is transformed to a discretized form of wave equation following the incorporation of grad div term [6] and symmetrical formulation [7], given by 2.2, that describes the EM fields inside the enclosure of a rectangular box containing the structure under consideration and thereby defining a boundary value problem (see Appendix 7.1). In this matrix form of the discretized wave equation, $\vec{e}$ is a vector that contains the electric field components for all mesh cells. The system matrix M contains all the information about the material properties, dimensions and frequency. $\vec{b}$ represents in general the source for the excitation through waveguide ports or internal ports. In case of the waveguide ports, $\vec{b}$ corresponds to the sum over all transversal electric fields of the available modes at the waveguide ports.

$$\nabla \times \nabla \times \vec{E} - k_0^2 \vec{E} = \mathbf{0} \tag{2.1}$$

$$M\,\vec{e} = \vec{b} \tag{2.2}$$

It is worth to look into the construction of the matrix wave equation closely. The F3D solver based on the FDFD method is developed according to a Cartesian coordinate system where all the information of the materials, dimensions etc. as well as fields and sources are assigned to the matrix and vector elements, respectively, cell by cell, first of all in the x direction, then in the y direction and lastly in the z direction as given by the equation of 2.3. M_{ij}'s (i, j = x, y, z) are the sub matrices with dimension of $n \times n$, where n is the size of the mesh, and $\vec{e}_i$'s as well as $\vec{b}_i$'s are the vectors with dimension n. A more comprehensive representation of 2.3 is given by 2.4 where $a_{i,j}$'s are the elements of matrix M consisting of material and dimensional information, e_i and b_i (i = 1 ... $3n$) represent the field and source components corresponding to the vectors $\vec{e}$ and $\vec{b}$, respectively. It should be noted that M is symmetric but not positive definite and consists only of very few diagonals with nonzero elements.

$$\begin{bmatrix} M_{xx} & M_{xy} & M_{xz} \\ M_{yx} & M_{yy} & M_{yz} \\ M_{zx} & M_{zy} & M_{zz} \end{bmatrix} \cdot \begin{bmatrix} \vec{e}_x \\ \vec{e}_y \\ \vec{e}_z \end{bmatrix} = \begin{bmatrix} \vec{b}_x \\ \vec{b}_y \\ \vec{b}_z \end{bmatrix} \tag{2.3}$$

$$\begin{bmatrix} a_{1,1} & .. & .. & a_{1,3n} \\ .. & .. & a_{i,j} & .. \\ .. & .. & .. & .. \\ a_{3n,1} & .. & .. & a_{3n,3n} \end{bmatrix} \cdot \begin{bmatrix} .. \\ e_i \\ .. \\ e_{3n} \end{bmatrix} = \begin{bmatrix} .. \\ b_i \\ .. \\ b_{3n} \end{bmatrix} \tag{2.4}$$

The matrix equation of 2.4 is solved for the unknowns of e_i with an iterative numerical algorithm, namely a Krylov-subspace method [10, 15] with the Independent Set Ordering and SSOR-preconditioning procedure (see the Appendix 7.7). In this procedure the values of the unknowns are updated as long as the unknowns converge to a predefined tolerance.

As the anisotropic PML satisfies Maxwell's equations, the PML cells become part of the bounded region automatically during the discretization. The influence of these anisotropic PML cells on the convergence of the iterative solution can be explained with the help of the Gerschgorin circles [45]. The union of the Gerschgorin circles of radius r_i contains all the eigenvalues of the system matrix M, where the radius r_i is calculated as the summation of the magnitudes of all the non-diagonal elements of the i^{th} row in M given by 2.5. A quantity ρ_i is defined as the ratio between the summation of the magnitudes of all the non-diagonal elements and the diagonal element at the i^{th} row in M according to equation 2.6. Again $\rho_{\max}$ is the maximum value of ρ_i considering all the rows of the system matrix M given by the equation 2.7. Some examples of Gerschgorin circles are shown in Fig. 2.1.

$$r_i = \sum_{\substack{j=1 \\ j \neq i}}^{3n} | a_{i,j} | \tag{2.5}$$

$$\rho_i = \frac{r_i}{| a_{i,i} |} \tag{2.6}$$

$$\rho_{\max} = \max_{1<i<3n} \{ \rho_i \} \tag{2.7}$$

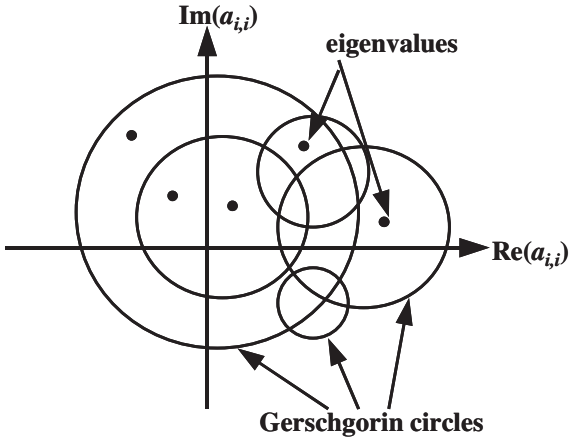

Fig. 2.1 Gerschgorin circles with centers at (Im($a_{i,i}$), Re($a_{i,i}$)).

For M to be a positive definite matrix, ρ_i must be smaller than one, all the eigenvalues must lie within the right hand side of the imaginary axis in order to make the iterative solution provide a stable convergence. But in the case of FDFD method, M is usually not a positive

definite matrix, i.e. the periphery of the circles with some of the eigenvalues extends to the left hand side of the imaginary axis which may lead to a bad convergence.

In order to describe the importance and consequences of the parameters of r_i, a_{ii} and ρ_i for the numerical convergence of the FDFD method with PML the patch antenna[19] in Fig. 2.6.a is examined. It is assumed that the antenna has only one PML (X-PML) boundary followed by a magnetic wall in the direction perpendicular to the patch. Other open boundaries are terminated by magnetic walls. Under these conditions the antenna is simulated at 16 GHz and the parameters r_i, a_{ii} and ρ_i are calculated out of the system matrix at each row. The same is done for the case with the PML medium replaced by air while keeping the discretization scheme the same, this is termed as the case without PML (no PML). The ratios between the cases of with PML and without PML for all these three parameters are calculated. In each case the ratios which are equal to one, corresponding to the inner mesh cells and rows of the system matrix not affected by the PML medium, are excluded. The remaining ratios are sampled linearly (counted in stepped ranges) and drawn in Fig. 2.2.

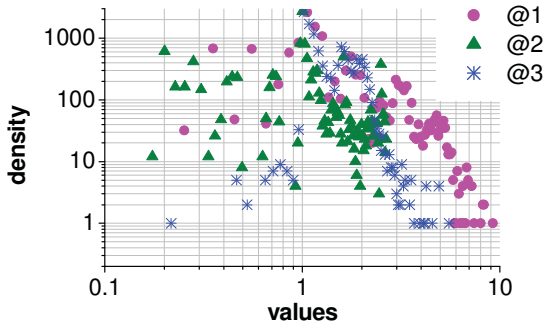

$$@1: \frac{r_i^{pml}}{r_i^{no\ pml}},\quad @2: \frac{|a_{ii}^{pml}|}{|a_{ii}^{no\ pml}|},\quad @3: \frac{\rho_i^{pml}}{\rho_i^{no\ pml}}$$

Fig. 2.2 Densities of the values given by the ratios of @1, @2 and @3. The total number of rows in M is 75816 (=3×27×36×26) and the number of the PML affected rows where the ratios given by @1, @2 and @3 are not equal to one is 12273.

Looking at Fig. 2.2, it is evident that introducing the PML results in an increased number of rows in M where the values of the ratios defined by @1, @2 and @3 are larger than 1.0. In addition, the values of @1 are larger than those of @2. This helps to state that the addition of the PML wall increases the values of ρ_i and correspondingly ρ_{max}, which means that the radii of the Gerschgorin circles become larger and the possibility of the real parts of the eigenvalues to be more negative increases. The outcome is that the condition number grows larger and the convergence of the iterative process is more unstable when the PML wall is included. In this way the inclusion of the PML wall results in a change in the numerical properties of the system matrix and thereby affects the convergence of the solver, i.e., the number of iterations. The number of iterations is taken here as a measure for the numerical efforts and it is directly proportional to the CPU time needed to obtain the solution.

When discussing the numerical consequences of introducing the PML, it is important to have a close look on the resulting permittivity and permeability tensors, which are written here as the products of the isotropic physical material constants and a tensor [**η**] representing the PML properties according to [3, 4] (see equations (2.8) and (2.9)). [**η**] is a diagonal tensor with the complex parameter η_i, the imaginary part of which defines the attenuation and thus the residual reflections at the PML (see Fig. 2.3). The nominal reflection coefficient (r_{th}) of equation 1.1 can be written in terms of the imaginary part of η_i ($\mathrm{Im}(\eta_i)$) as 2.10. As attenuation and reflection are inversely proportional, attenuation (α_{th}) can be written as 2.11. For low reflection, i.e., high attenuation in the PML, the product of $|\mathrm{Im}(\eta_i)|$ and d must be large. On the other hand, $|\mathrm{Im}(\eta_i)|$ should not be too large, as the matrix condition depends on $\mathrm{Im}(\eta_i)$. So for higher attenuation as well as better matrix condition a relatively small $|\mathrm{Im}(\eta_i)|$ and large d should be chosen. When using PML walls for several outer boundaries, these walls overlap at edges and corners as illustrated in Fig. 2.3. In case of the overlapping at the edges (e.g. overlapping 1 & 2) and corners (overlapping 1, 2 & 3) the resulting PML tensor is the product of the PML tensors of the individual PML walls that form the edges and corners, respectively.

$$[\bar{\boldsymbol{\varepsilon}}] = \varepsilon_0 \varepsilon_r [\bar{\boldsymbol{\eta}}] \tag{2.8}$$

$$[\bar{\boldsymbol{\mu}}] = \mu_0 \mu_r [\bar{\boldsymbol{\eta}}] \tag{2.9}$$

$$r_{th} = \exp\left(\frac{-2\sqrt{\varepsilon_r}\,\omega\,|\,\mathrm{Im}(\eta_i)\,|}{(p+1)\,c_0} d \right) \tag{2.10}$$

$$\alpha_{th} \propto \omega \cdot |\,\mathrm{Im}(\eta_i)\,| \cdot d \tag{2.11}$$

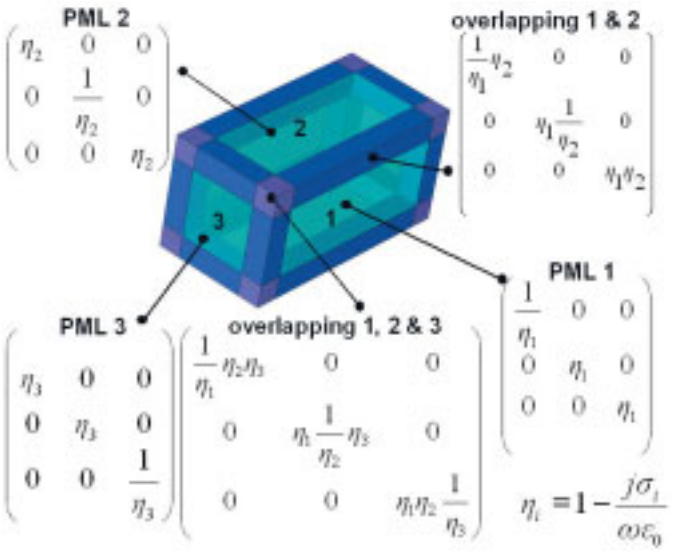

Fig. 2.3 PML Tensors [**η**] (see equations (2.8) and (2.9)) for PML walls in three directions detailing the overlapping regions. σ_i denotes the artificial conductivities (electrical) of the respective PML wall as derived from a given nominal reflection factor (equation 1.1).

The inspection of the tensors according to Fig. 2.3 reveals that, because always both η_i and its inverse appear, the PML increases the magnitude range of the material tensors and thus that of the resulting entries in the system matrix, which in turn increases the radii of the Gerschgorin circles as mentioned above. As these circles contain all the eigenvalues of the system matrix, larger radii of those circles means higher possibilities of the real parts of the eigenvalues to assume smaller values and thereby worse convergence. This situation becomes particularly critical for the overlapping regions since there several factors of the η_i are multiplied. In order to demonstrate this, Tab. 2.1 shows typical values for the PML tensor elements (based on an example at 1GHz with –60dB nominal reflection). This is the basic effect why PML causes the numerical properties to deteriorate but one needs an in-depth investigation to better understand the underlying effects and to find the solutions minimizing the odds. This is presented in the following sections.

$\lvert\eta_1\rvert$	$\lvert 1/\eta_1\rvert$	$\lvert\eta_2\rvert$	$\lvert 1/\eta_2\rvert$	$\lvert(1/\eta_1)\eta_2\rvert$	$\lvert\eta_1\eta_2\rvert$	$\lvert(1/\eta_1)\eta_2\eta_3\rvert$	$\lvert\eta_1(1/\eta_2)\eta_3\rvert$
83.0	0.012	75.0	0.013	0.9	6225	67.5	83

Tab. 2.1 Diagonal elements of PML tensors according to Fig. 2.3 (ε_r of PML wall 1 and 2 are 1.0 and 2.2 respectively; σ_i of PML wall 1 and 2 are 4.6 and 4.2 respectively; μ_r is 1.0 in all cases; for calculation of σ_i see [18, 19]).

Having known that PML in general worsens the convergence of the iterative solution it is investigated quantitatively which parameters of the PML wall affect the convergence mostly and how that can be tempered by modifying the PML regions and parameters. The most vital modifications and parameters will be discussed separately following some general considerations regarding convergence as given below:

1. As already mentioned in chapter 1, the interface of the PML/non PML regions in the discretized description of FDFD method results in spurious reflections. This mismatch problem can be alleviated by subdividing the PML region into a number of layers with varying conductivity [19]. In this point it is important to know the impact of the number of PML layers on the convergence. More layers improve of course the accuracy but increase the numerical expenses. It is found that a 5-layer configuration provides a good compromise and this number is used in all the following investigations.

2. The convergence of the iterative solver is influenced also by the choice of the PML backing. Commonly, PML walls are followed by electric or magnetic walls. We found that for the structures considered in this work, electric walls lead to a less number of iterations than magnetic walls.

3. Adjacent PML and non-PML cells should have sizes of comparable dimensions to have the results less erroneous and iterations reduced in number.

4. The number of iterations increases with the increase in $|\varepsilon_{max} - \varepsilon_{min}|$ and frequency, where ε_{max} and ε_{min} are largest and smallest relative dielectric constants within the structure. These are general characteristics of the FDFD simulation, independently whether PML is included or not.

2.2 Overlapping PML Walls

While for a single PML wall the tensor elements are in the range $1/\eta \ldots \eta$, this becomes worse if overlapping regions of two PML walls are included. Assuming that both PML walls have the same properties, the tensor elements within the structure now cover the range $1/\eta \ldots 1 \ldots \eta^2$. Proceeding with 3 overlapping PML regions the overall situation does not change from this point of view because the additional elements are of same order (if one assumes identical PML properties). To give numbers, Tab. 2.1 shows that for a single PML wall (e.g. PML wall 1) the range of tensor elements is (0.012 - 83.0) and when the PML wall 2 is included the range of matrix elements extends to (0.012 .. 6225.0).

Going beyond these relatively simple arguments, extensive investigations were performed simulating typical microwave structures with different PML configurations. It is found that the PML disposition indeed has a drastic influence on the efforts required for solving the system of equations. Introducing a single PML wall already leads to a significant increase in the number of iterations of the solver (typically a factor of 2). Including overlapping regions with 2 PML results in further drastic deteriorations (an additional factor >15), which in many cases render this approach useless for practical design work. Adding more PML walls with overlapping regions, convergence deteriorates further.

It is found that this deterioration of convergence can be alleviated by modifying the PML definition in the edge and corner regions. Different ideas have been tested including an angle-dependent description and the insertion of additional physical conductivities in the PML formulation for numerical stabilization. All these approaches did not yield the desired improvements. The best solution turned out is to avoid any overlapping. Avoiding the overlapping PMLs is carried out by disjoint PMLs (called non-overlapping PML) where the edges and corners are replaced by the complete PML walls. Since the edges and corners form only a very small fraction of the overall PML surface, the reflections occurring there remain negligible in most cases and one can use a PML with attenuation in a single direction instead. Fig. 2.4 illustrates this idea of non-overlapping PML for the edge case. When PML 1 overrides PML wall 2, it is referred to as “12” orientation in the following and vice versa.

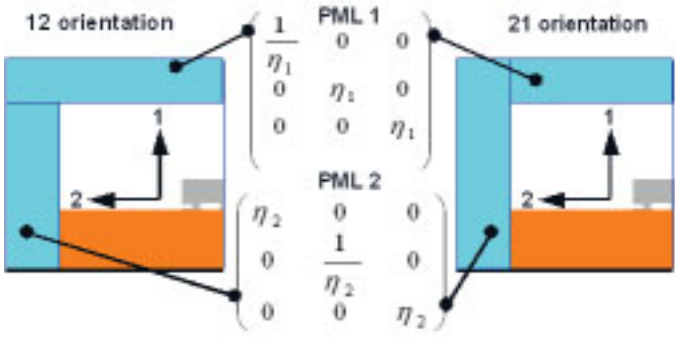

Fig. 2.4 Edge of the structure according to Fig. 2.3 with non-overlapping (disjoint) PML walls illustrating 2 possibilities of edge description.

This approach to circumvent the problem with overlapping PMLs proves its effectiveness for various structures like patch antenna, microstrip, flip-chip or LTCC structures. The

investigations of how the inclusion of PML (overlapping) and non-overlapping PML influences the matrix elements, and thereby the convergence of the iterative solution will be presented in the following dealing a micro-strip line and a patch antenna.

The micro-strip structure of Fig. 2.5.a is simulated at 20 GHz first of all without any PML wall. In order to keep the mesh the same for all the simulations, the PML walls are not just excluded from the structure, rather the tensor elements of the PML walls are made unity (η = 1.0) in order to represent the case without PML. In this case the PML cells are there but not filled with PML material. The density distribution of the non-zero matrix elements as a function of magnitudes is shown in Fig. 2.5.b.

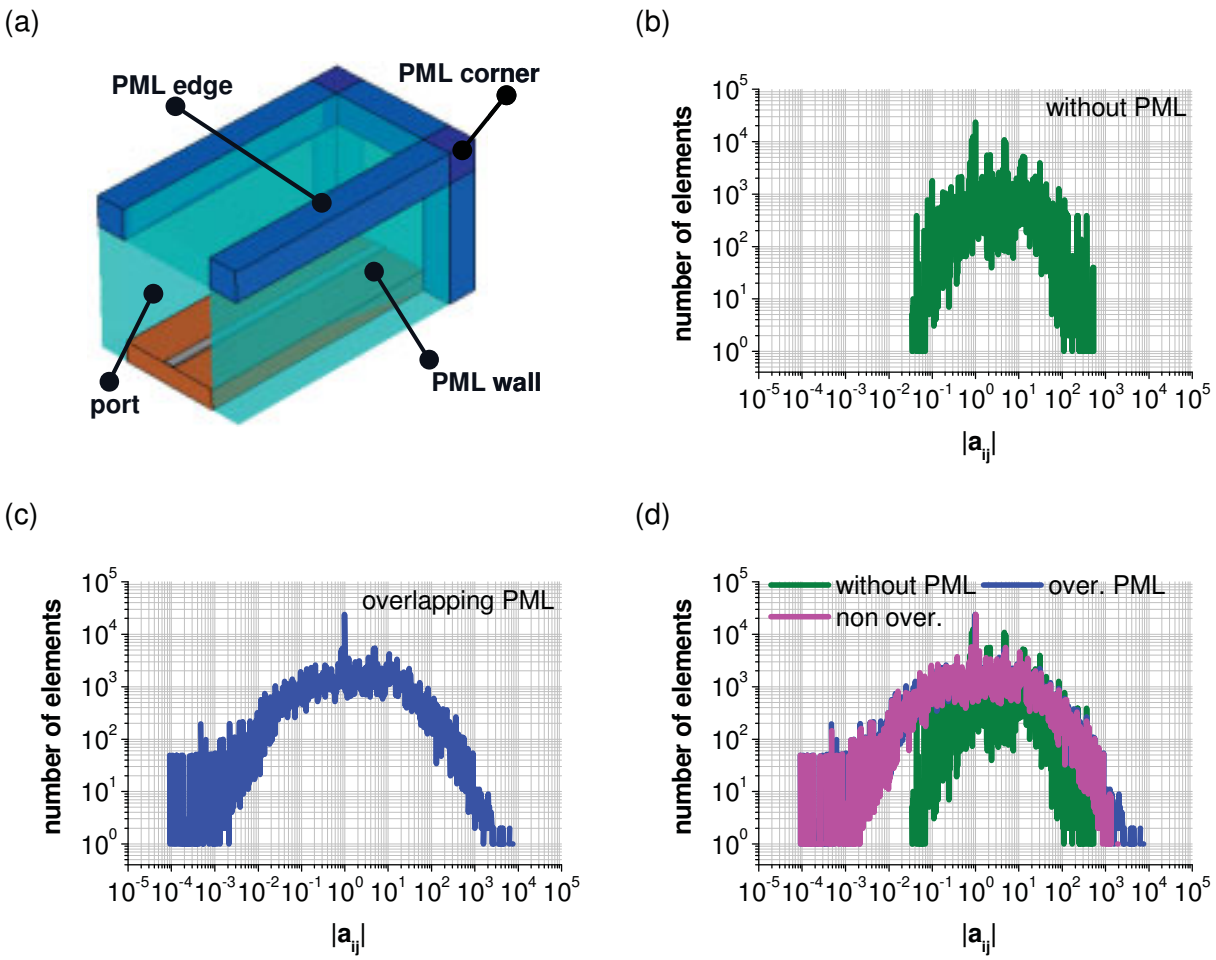

Fig. 2.5 a) The micro-strip (MS) surrounded by PML walls on all sides other than the port. The MS is 10 µm thick and 50 µm wide. The substrate (ε_r = 9.8) is 100 µm thick. The PML walls consisting of 5 layers with variable thicknesses have an overall reflection error of -70dB and parabolic spatial variation of the conductivities.

The density of the matrix elements a_{ij} in relation to their magnitudes for the case without PML walls (b), with PML walls including the overlapping regions (c) and with non-overlapping PML walls (d). In (d) graphs in (b) and (c) are redrawn for comparison. The lowest and largest values of the magnitudes are in (b) 1.74E-02 and 845.62, in (c) 7.54E-05 and 7584.38, and, in (d) 7.4E-05 and 1994.16 respectively.